npj | climate and atmospheric science

Article

Published in partnership with CECCR at King Abdulaziz University

https://doi.org/10.1038/s41612-024-00694-2

Hemispherical scale mechanisms of nitrate formation in global marine aerosols

Qibin Lao[1], Hongliang Li[2], Jinpei Yan[3], Guangzhe Jin[1,4], Guirong He[1], Chunqing Chen[1], Qingmei Zhu[1,4] & Fajin Chen[1,4]

Nitrogen oxides (NO_x) in the atmosphere directly affect air quality; however, their oxidation products (e.g., nitrate) are essential nutrients in terrestrial and marine ecosystems. To date, the mechanism and rate of nitrate formation in the global-scale marine boundary layer remains uncertain. Herein, aerosol nitrate isotopes covering the global ocean were analysed and observations indicated that nitrate formation was dominated by the proportion between the hydroxyl radical (daytime) and ozone (nighttime) pathways in the Northern Hemisphere (NH), whereas it changed to the BrO (Antarctic iceberg emission) pathway in the Southern Hemisphere (SH). These differences in the pathways suggested that the NO_x removal (nitrate formation) efficiency was higher in the NH, which could be responsible for the much higher nitrate concentrations in the NH than in the SH (over twice). This study can assist in formulating effective policies to mitigate global NO_x pollution and improve our understanding of the impact of increasing NO_x concentrations on global ocean productivity.

Nitrogen oxides ($NO_x = NO_2 + NO$) are essential for the formation of secondary atmospheric aerosols and atmospheric oxidants, including ozone (O_3) and hydroxyl radicals (OH), which control the self-cleaning capacity of the atmosphere[1]. Although NO_x emissions have generally decreased in Europe and North America owing to effective control measures[2,3], they continue to increase in most regions (such as East and South Asia) because of intensive anthropogenic activities[4–6], resulting in a substantial elevation in global atmospheric nitrogen deposition over the last 100 years[7]. Nitrate (NO_3^-), an essential nutrient in terrestrial and marine ecosystems, is the main oxidation product of NO_x and is therefore considered its primary sink[8]. After NO_x is converted into NO_3^- in the atmosphere, it can enter surface and marine environments through dry and wet deposition, significantly impacting land and marine productivity and carbon biological pumps[9,10]. The ocean is the largest active carbon reservoir on Earth, with enormous carbon sequestration potential[11,12]. Atmospheric nitrogen deposition has been widely demonstrated to play an extremely important role in global ocean productivity and biochar pumping, especially under global warming[9,13,14]. The contribution of atmospheric nitrogen deposition becomes more significant because warming strengthens ocean stratification, decreasing nutrient supply from deep water to the upper ocean[15]. However, the mechanism and rate of NO_3^- formation in the global-scale marine boundary layer remain uncertain, which greatly limits our ability to predict the effects of the lifetimes of NO_x and their oxidation products on marine ecology and global climate change.

Atmospheric NO_x and its derived nitrogen-compounds deposited on the ocean surface originate mainly from continents[16,17] as direct NO_x emissions from the ocean are negligible[1]. Therefore, comprehensively understanding the fate of NO_x over the marine atmospheric boundary layer (MABL) is critical, which can not only develop more effective mitigation strategies but also further evaluate the impact of their oxidation products on marine ecosystems. Several oxidation pathways act for NO_3^- formation from NO_x in the atmosphere (Supplementary Text 1). Globally, ozone (O_3) and hydroxyl radical (OH) oxidation are the two dominant pathways that convert NO_x to NO_3^-, and account for approximately 41% of the total NO_3^- generation[18,19]. In addition, other oxidants such as BrO, hydrocarbons (HC), and dimethyl sulphide (DMS) are regionally important[19]. On a global scale, the distribution of these oxidations is non-uniform, particularly between the northern (NH) and southern (SH) hemispheres[20,21]. Furthermore, NO_x oxidation differs between daytime (mainly by OH) and night-time (mainly by O_3, HC, and DMS). Day length directly affects the formation of OH in the atmosphere and is an important factor affecting atmospheric NO_3^- formation[22]. Thus, the NO_3^--formation pathways may differ in the two hemispheres. In addition, the NO_3^- formation efficiencies of different pathways vary greatly, with a higher OH production rate[20,23]. Therefore,

[1]College of Ocean and Meteorology, Guangdong Ocean University, Zhanjiang, China. [2]Key Laboratory of Marine Ecosystem Dynamics, Second Institute of Oceanography, Ministry of Natural Resources, Hangzhou, China. [3]Key Laboratory of Global Change and Marine Atmospheric Chemistry, Ministry of Natural Resources, Xiamen, China. [4]Key Laboratory of Climate, Resources and Environment in Continental Shelf Sea and Deep Sea of Department of Education of Guangdong Province, Guangdong Ocean University, Zhanjiang, China. e-mail: fjchen@gdou.edu.cn

understanding the mechanisms controlling NO_3^- formation pathways in the global MABL can deepen our understanding of the impact of increased anthropogenic NO_x emissions on global marine primary productivity and oceanic CO_2 sinks.

The oxygen isotope of nitrate ($\delta^{18}O$-NO_3^-) provides original information on the nature and relative importance of NO_x oxidation pathways for NO_3^- formation[24]. Usually, the NO_3^- produced via the OH pathway is characterised by negative $\delta^{18}O$-NO_3^- as one-third of oxygen atoms in formed NO_3^- comes from OH, which characterises negative $\delta^{18}O$ (−15~0‰)[25]. NO_3^- formed via the O_3 pathway has higher $\delta^{18}O$ because five-sixth of the oxygen atoms in two formed NO_3^- come from O_3 (90~120‰)[26]. In addition, NO_3^- formed via BrO, DMS, or HC exhibits the highest $\delta^{18}O$ since these processes originate from the terminal oxygen atom of O_3 (~130‰)[17]. Therefore, the composition of $\delta^{18}O$-NO_3^- depends on the relative importance of these oxidants in NO_x oxidation, enabling researchers to identify and apportion NO_x sinks[27]. Herein, we conducted a total of eight cruises covering the Pacific, Indian, Atlantic, Arctic, and Southern Oceans to analyse aerosol NO_3^- and its oxygen isotope ($\delta^{18}O$-NO_3^-) in the MABL to present a comprehensive understanding of the NO_3^- formation mechanism (removal of NO_x) over the global ocean.

Results

Characteristics of NO_3^- and $\delta^{18}O$-NO_3^- in global marine aerosols

For the Indian Ocean, Northwest Pacific Ocean, and Arctic cruises, NO_3^- concentrations and $\delta^{18}O$-NO_3^- compositions ranged from 0.5 to 217.0 nmol m^{-3} and 53.3 to 91.8‰, respectively (Supplementary Table 1). Globally, the aerosol NO_3^- concentrations have wide variation (0.2–467.2 nmol m^{-3}), with a higher concentration around the coastal areas, particularly in marginal seas of Asia and Europe, and lower concentrations in the open oceans and polar regions (Fig. 1a). Generally, aerosol NO_3^- concentration in the MABL is higher in the NH (23.9 ± 46.3 nmol m^{-3}), which is more than twice that of the SH (10.9 ± 18.3 nmol m^{-3}) (Fig. 2a).

$\delta^{18}O$-NO_3^- values varied greatly over the global MABL (Fig. 1b). In the NH, the $\delta^{18}O$-NO_3^- values generally decreased with latitude, with a significant trend from the mid (30°N) to high latitudes (Fig. 2). The high $\delta^{18}O$-NO_3^- values occurred in the Northwest Pacific Ocean (mid-low latitudes), and the values gradually decreased toward high latitudes in the Arctic, with low values in the Arctic regions. However, the $\delta^{18}O$-NO_3^- values showed a different trend in the Eastern Pacific and Atlantic Oceans, with latitudinal increases and low values appearing in the mid-eastern Pacific Ocean (Fig. 1b). The difference in the trend of $\delta^{18}O$-NO_3^- values in the MABL of NH may be related to the sampling period, which directly determines the major pathway of NO_3^- formation. Conversely, the $\delta^{18}O$-NO_3^- values generally exhibited lower values in the low latitudes whereas high values in the high latitudes (Fig. 1b), with a significantly increased trend with latitude (Fig. 2). Additionally, the $\delta^{18}O$-NO_3^- value in the Southern Ocean (an average of 73.5 ± 7.7‰) is remarkably higher than in the Arctic Ocean (an average of 61.0 ± 5.0‰), reflecting the difference in the oxidants that influence the formation of NO_3^- between these two polar regions.

Discussion

The obvious difference in variations of $\delta^{18}O$-NO_3^- values between the NH and SH (Fig. 2) reflected different NO_3^- production pathways. In the NH, unlike the variation of $\delta^{18}O$-NO_3^- values (Fig. 2), the distribution of O_3 exhibited a decreased trend from higher latitudes to the tropics (Supplementary Fig. 1). Although the O_3 values exhibited significant seasonal changes, the decoupling of $\delta^{18}O$-NO_3^- and O_3 (Fig. 3a) suggested that the O_3 value and its seasonal variation were not the major factors controlling NO_3^- formation. Similarly, BrO concentrations generally increase with latitude in both the NH and SH[20,28]. However, although enhanced BrO occurs in the polar regions, the BrO levels in the high-latitudes of the Arctic are much lower than that of the high-latitudes of the Antarctic[28,29]. Therefore, BrO is unlikely to be the major factor controlling NO_3^- formation in the NH. This is also supported by the decoupling of $\delta^{18}O$-NO_3^- and tropospheric BrO column in the NH (Fig. 3c). Nevertheless, regionally, the BrO pathway can be important for NO_3^- production[19]. For example, modelling results have shown that BrO concentrations in the eastern North Pacific and northern North Pacific are higher than those in other regions of the Pacific[20], and NO_3^- generation via the BrO pathway is responsible for the higher

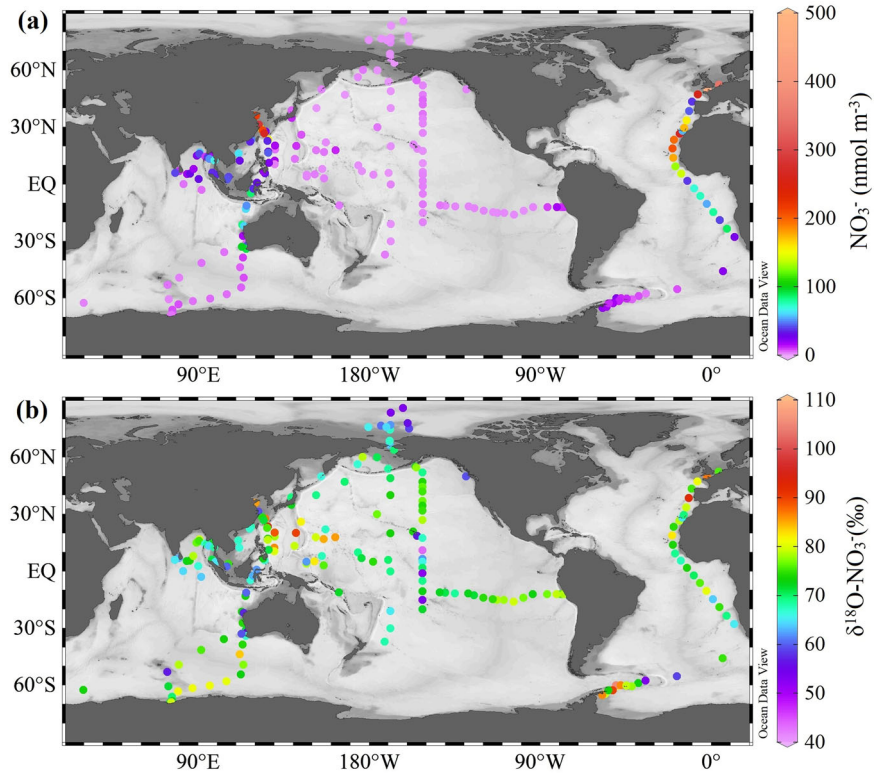

Fig. 1 | The distribution of NO_3^- concentration and its isotopic composition in the global ocean. Panels **a** and **b** show the distribution characteristics of aerosol NO_3^- concentrations and $\delta^{18}O$-NO_3^- values in the global ocean, respectively.

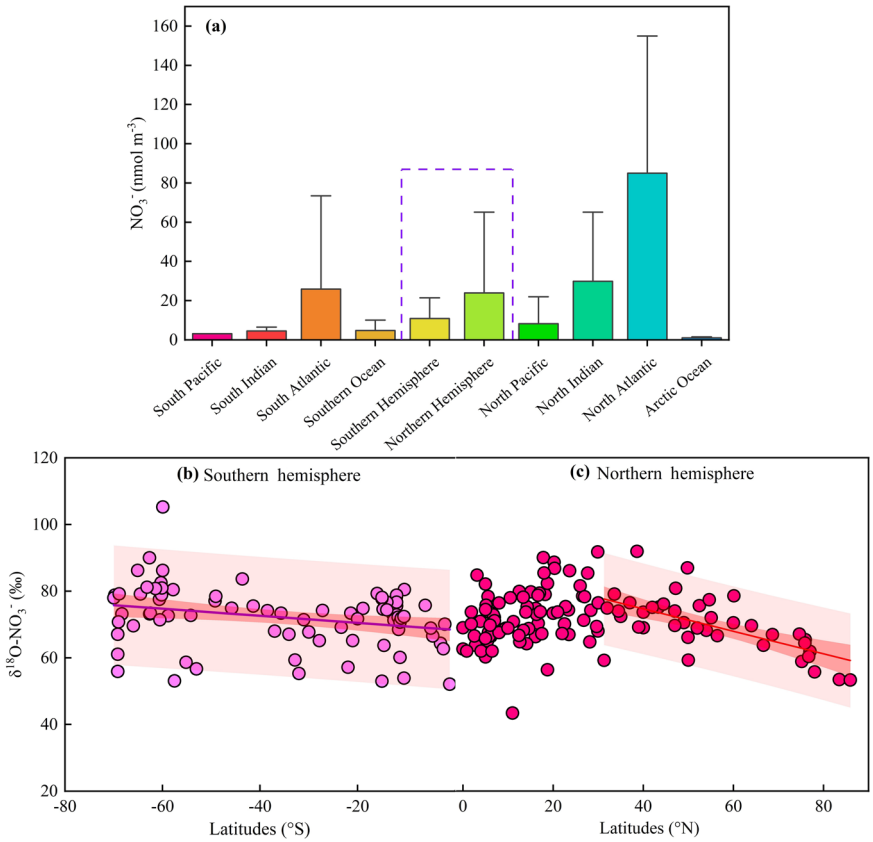

Fig. 2 | Characteristics of NO_3^- and its oxygen isotope in oceanic aerosols from the Northern and Southern Hemispheres. The purple dashed line in **a** marks the mean value of the Northern Hemisphere and Southern Hemisphere. **a** Samples with latitudes higher 60° S represent the Southern Ocean, samples with latitudes higher 65° N represent the Arctic ocean, and other oceanic regions are aerosol samples covered by their respective regions in Supplementary Fig. S5. Solid lines in **b** and **c** represent the linear regressions, the light pink backgrounds represent the 95% Prediction Band, and the dark pink backgrounds represent the 95% Confidence Band.

δ^{18}O-NO_3^- values in these regions[30]. However, this is not the case in the western North Pacific. As the lowest BrO concentration occurred in the western North Pacific[20], higher δ^{18}O-NO_3^- values were observed in this region (Fig. 1b).

NO_3^- formation via the OH pathway likely dominated that of NH. The OH concentrations in the atmosphere mainly depend on the length of the day (duration of formation through daytime and night-time reactions) because the OH is a photolytic product[31,32]. Thus, OH formation exhibits seasonality proportional to the solar radiation intensity (day length), and OH concentrations in the tropics are remarkably higher than those in the polar regions[21]. Additionally, the OH concentration exhibited a remarkable decrease from summer to winter owing to weaker solar radiation and shorter day length in winter[21]. However, after corresponding to the sampling date, the δ^{18}O-NO_3^- value exhibited a significantly negative correlation with day length (Fig. 3e), suggesting that a longer day length and more substantial solar radiation favour the formation of a lower δ^{18}O in NO_3^- (mainly via the OH pathway). In the Arctic, the sampling data during summer was on permanent daytime (Supplementary Fig. 2), which completely inhibited the night-time reaction (O_3 pathway) owing to the photolytic sensitivity of NO_3^-[17]. During this period, the suppressed night reaction (O_3 pathway) and dominant day reaction (OH pathway) were responsible for the low δ^{18}O-NO_3^- value in the Arctic regions[18]. Contrarily, the Northwest Pacific Ocean cruise occurred in winter, during which the day length was shorter, and solar radiation was weaker, favouring the formation of NO_3^- via the O_3 pathway[18].

Night-time reactions play a key role in the reactive nitrogen budget, and this process is important at the Intertropical Convergence Zone (ITCZ) boundary of the NH because of the large aerosol surface area during N_2O_5 hydrolysis[24]. Moreover, nocturnal oxidation driven by nitrate radicals has significantly increased over continents off the Northwest Pacific[33]. Therefore, NO_3^- formed mainly via the O_3 pathway could be responsible for the higher δ^{18}O-NO_3^- values observed during this period (Fig. 1b). However, although the Indian Ocean cruise was conducted in winter, the latitude was lower than that of the Northwest Pacific Ocean cruise, indicating that the Indian Ocean cruise had a longer day length and higher solar radiation. Thus, δ^{18}O-NO_3^- values in the northern Indian Ocean (an average of 69.1 ± 5.0‰) are lower than those in the Northwest Pacific Ocean (an average of 81.9 ± 7.3‰). Similarly, the sampling dates of the eastern Pacific Ocean-G15 cruise are in late spring to early winter, during which the day length decreases with the latitude (Supplementary Fig. 2), reflecting an increased proportion of NO_3^- formation via the O_3 pathway (an increase of δ^{18}O-NO_3^- value with latitude, Fig. 1b). Overall, day length was the dominant factor controlling NO_3^- formation in the NH.

In the low latitudes (0−30°S) of the SH, δ^{18}O-NO_3^- values were lower, except in the eastern Pacific (Fig. 1b). Along the longitude (similar day length, 13.8 − 14.5 h) in the eastern Pacific Ocean-G16, the proportion of NO_3^- formation via the OH pathway is similar, and the variation of δ^{18}O-NO_3^- value may depend on the distribution of marine alkyl nitrate and O_3[34]. However, both O_3 and BrO concentrations are low in the low latitudes[20], suggesting that the NO_3^- formation by the oxidation of O_3 and BrO is minor in these regions. The lower δ^{18}O-NO_3^- values could be affected by the dominance of the OH reaction pathway due to the high OH concentration in these regions[21]. A quantitative estimation showed that the OH pathway contributes up to 80 ± 5% of the NO_3^- formation in the tropical MABL of the Pacific Ocean in the SH[17]. The O_3 pathway is unlikely to be a factor in elevating the δ^{18}O-NO_3^- value at mid-high latitudes. The higher O_3 concentration occurred in the mid-latitudes (30 − 60°S), whereas the concentration in the high latitudes (>60°S) was even lower than that in low latitudes (Supplementary Fig. 1), which differs from the distribution of δ^{18}O-NO_3^-. In addition, most sampling activities were conducted under sunlight conditions (long day length) at high latitudes, which are not favourable for NO_3^- formation via the O_3 pathway. No correlation was observed between the δ^{18}O-NO_3^- value and the O_3 concentration or day length in the SH (Fig. 3). However, the BrO concentration increased remarkably from approximately 30°S toward the polar regions, with an extremely high concentration in the polar regions[20]. Correspondingly, the

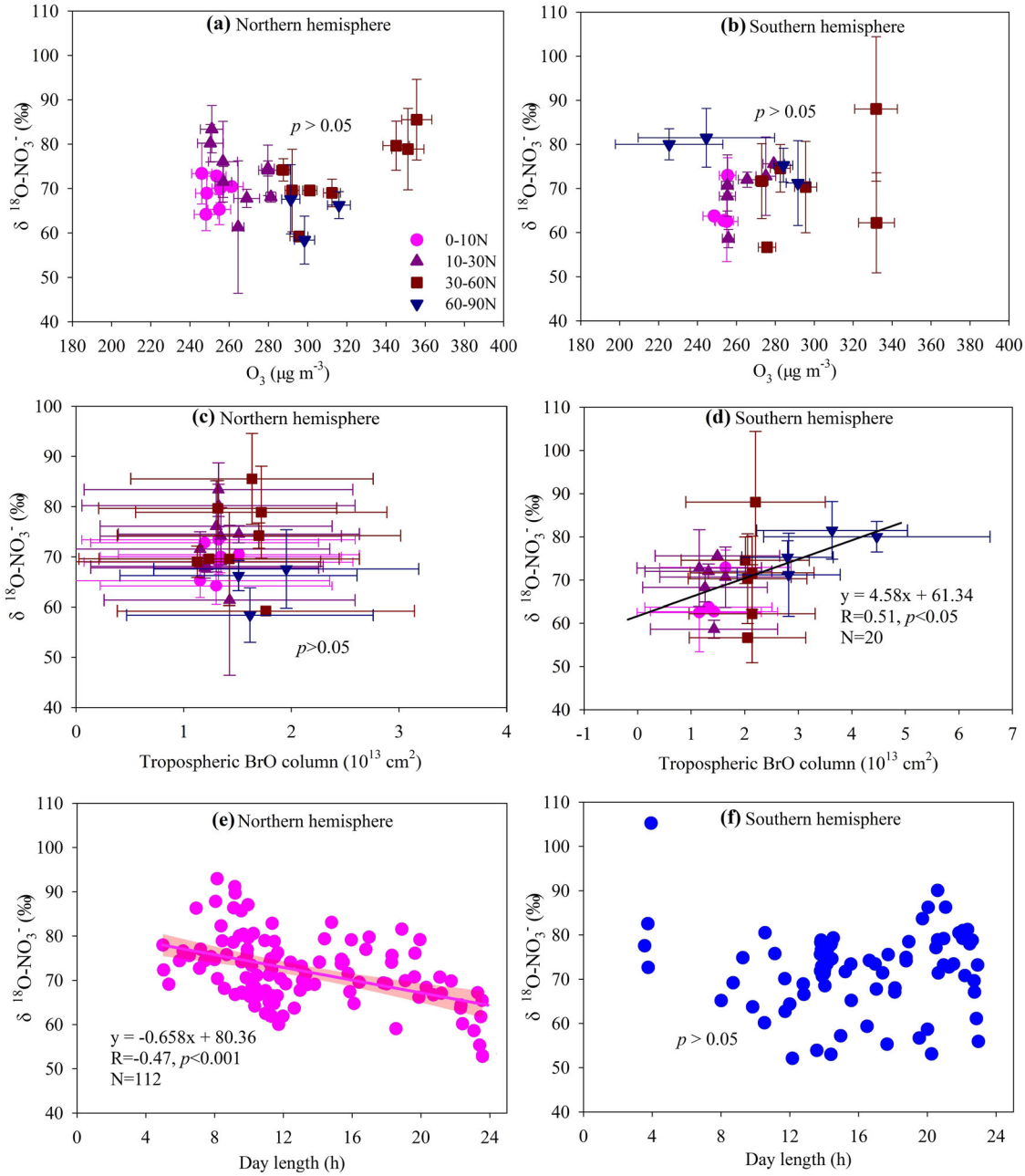

Fig. 3 | Correlation of $\delta^{18}O\text{-}NO_3^-$ values with ozone, BrO and day length in the Northern and Southern Hemispheres. Panels **a**–**f** show the relationship between $\delta^{18}O\text{-}NO_3^-$ and O_3 (**a** and **b**), BrO (**c** and **d**), and day length (**e** and **f**), respectively. The monthly average O_3 from 2006 to 2021 (the time range of all field observation cruises) for eight latitude bands (0–10°N, 10–30°N, 30–60°N, 60–90°N, 0–10°S, 10–30°S, 30–60°S, and 60–90°S) were obtained from National Aeronautics and Space Administration Ozone Watch (NASA Ozone Watch, https://ozonewatch.gsfc.nasa.gov/). The correlation between $\delta^{18}O\text{-}NO_3^-$ and O_3 is the average O_3 value in a certain latitude range (one out of the eight bands) in a specific month corresponds to the average $\delta^{18}O\text{-}NO_3^-$ value in that latitude range during that month. The monthly average BrO for eight latitude bands were obtained from the GOME-2 satellite instrument[28] and the data presented by Schmidt et al.[20]. Each sample corresponds to a day length value according to the sampling date and latitude. Solid lines represent the linear regressions and the light shading represents the 95% confidence intervals.

increasing trend of $\delta^{18}O\text{-}NO_3^-$ value in the mid-high latitudes (Fig. 1b) reflected the importance of NO_3^- formation via the BrO pathway in the mid-high SH[17,24]. This was also supported by the significant positive correlation between $\delta^{18}O\text{-}NO_3^-$ values and tropospheric BrO column in the SH after corresponding to the sampling month (Fig. 3d). Bromide ion concentrations in sea ice are approximately three times higher than those in seawater, and tropospheric BrO columns are usually enhanced in larger sea ice-covered areas[20,28]. Modelling predictions also suggest that NO_3^- formation via the BrO pathway is dominant at high latitudes in SH[19].

Unlike in the NH, the O_3 concentration was lower in the SH, decreasing significantly over the past few decades (Supplementary Fig. 1). In addition to anthropogenic influences[35], the level of NO_x can affect the production (polluted regions with a NO_x-rich atmosphere, mainly in the NH) and removal of O_3 (cleaner regions with a low-NO_x atmosphere, mainly in the SH) (Supplementary Text 2 and Supplementary Fig. 3). Although O_3 destruction in the SH causes a significant increase in the ultraviolet (UV) radiation at the Earth's surface, this is not conducive to OH formation. The primary generation of OH depends on the photolysis of O_3 by UV sunlight in the presence of water vapour[21]. In addition to the photodissociation of O_3, sources of OH generation, include the reactions of O_3 with terpenes emitted by vegetation, unsaturated hydrocarbons, and aromatic compounds in polluted air[21]. Thus, the OH concentrations in the

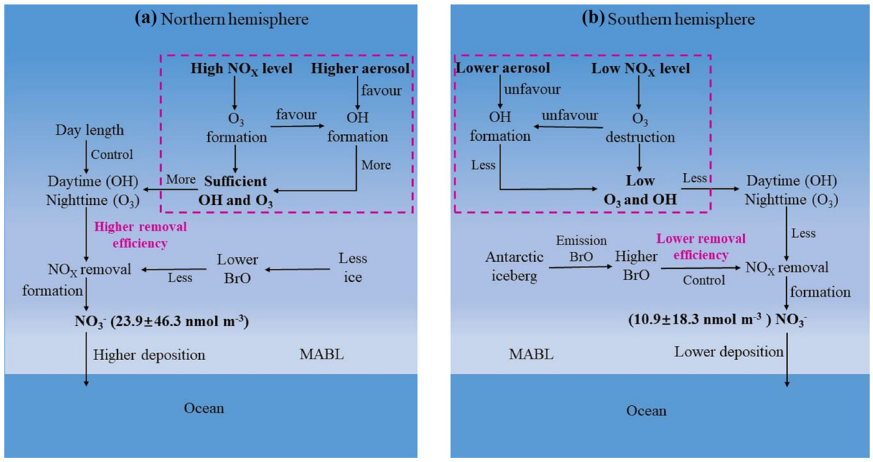

Fig. 4 | Schematics of aerosol NO_3^- formation mechanisms in the global ocean. Panels **a** and **b** show the aerosol NO_3^- formation mechanisms in the northern hemisphere and the southern hemisphere, respectively. MABL marine atmospheric boundary layer.

extratropical SH (6.6×10^5 molecules cm^{-3}) are remarkably lower than those in the extratropical NH (9.1×10^5 molecules cm^{-3})[21]. With sufficient OH and O_3, daytime (OH pathway) and night-time (O_3 pathway) reactions controlled by day length were the major pathways of NO_3^- formation in the NH. Although the seasonal variation in day length in the SH was consistent with that in the NH, O_3 loss and low OH concentrations led to less importance of daytime and night-time reactions in the mid-high latitudes of the SH. Moreover, particle size dramatically affects the NO_3^- formation mechanism[24]. The $\delta^{18}O$-NO_3^- value in the supermicron mode was significantly higher than that in the submicron mode. This is primarily because the OH pathway significantly affects NO_3^- in the submicron mode[24]. The aerosol optical depth in the NH was substantially higher than that in the SH (Supplementary Fig. 4) and was dominated by submicron-mode particles in the NH[36]. A recent study revealed that high concentrations of aerosol particles provide more expansive space for the reaction to generate OH, which then affects the formation of NO_3^-[24]. Combining these factors, the effect of the OH pathway on nitrate formation was more evident in the NH than in the SH.

According to the formation pathway of NO_3^- (R1-R7 in Supplementary Text 1), the theoretical values of $\delta^{18}O$-NO_3^- for different formation pathways can be calculated. Assuming that 2/3 of NO_3^--O originates from O_3 and 1/3 of O from OH in the OH pathway[37], the $\delta^{18}O$ value of NO_3^- formed by this pathway can be calculated to be 55‰ when the minimum $\delta^{18}O$ values of OH (−15‰) and O_3 (90‰) are chosen. Similarly, if 5/6 of NO_3^--O originates from O_3 and 1/6 of O from OH in the O_3 pathway[37], the maximum $\delta^{18}O$ value of NO_3^- is 100‰ using the maximum theoretical $\delta^{18}O$ values of OH (0‰) and O_3 (120‰). Since the NO_3^- formation via the BrO pathway is similar to that of terminal O_3, the maximum $\delta^{18}O$ value of NO_3^- formed by this way is 130‰. In this study, since the formation of NO_3^- in the NH is mainly controlled by the OH pathway (day length), the proportion of NO_3^- formed through this pathway can reach 60–100% (the theoretical minimum $\delta^{18}O$ value of the OH pathway divided by the measured value), reaching an average of 91% in the Arctic region. This is consistent with the nearly permanent daytime during the sampling period in Arctic[27]. At mid-high latitudes in the SH, since the BrO pathway is dominant for NO_3^- formation, the proportion of NO_3^- formed via this pathway ranges from 41% to 81% (the measured value divided by the theoretical maximum $\delta^{18}O$ value of the BrO pathway), reaching an average of 58% at higher latitudes (>60°S).

In addition to these three oxidants, other oxidants such as DMS and peroxy radicals can affect the atmospheric $\delta^{18}O$-NO_3^- value, this may introduce some uncertainty into our results. For instance, the low $\delta^{18}O$-NO_3^- value in the Arctic, besides being influenced by the day-length-controlled OH pathway, could also be partially attributed to the involvement of peroxy radicals (~23.9‰), as its O mainly originates from atmospheric O_2 rather than O_3[37]. Regionally, these oxidants may be important for NO_3^- production, and NO_x is inevitably affected by their oxidation during long-distance atmospheric transport to remote oceans. However, current research has shown that the impact of these factors on NO_3^- production is minimal on a global scale, with a contribution of less than 6%[18]. For local regions, fractionation during anthropogenic emissions cannot be denied and should not be overlooked, though their impact is comparatively small compared to natural oxidation pathways like OH, O_3 and BrO from a global perspective.

Differences in NO_x removal processes between the NH and SH can profoundly impact global tropospheric chemistry, such as secondary aerosol formation and oxidants[33]. The rate of OH-driven NO_x removal is much higher than that of NO_x removal by halogens (approximately 20% of the rate by OH)[20,23], which indicates that higher concentrations of NO_x in the NH correspond to higher removal efficiencies. Conversely, lower concentrations of NO_x in the SH correspond to lower removal efficiencies (Fig. 4). Low NO_x removal in the SH may gradually accumulate in the atmosphere, resulting in increased formation of new secondary aerosols in the clean atmosphere of remote Antarctica[38]. The high NO_x level and removal rate could be responsible for the much higher NO_3^- concentrations in the NH than in the SH (nearly twice). This suggests that the contribution of atmospheric nitrogen deposition to ocean productivity is more significant in the NH than in the SH. Model analyses have shown that global ocean productivity is declining[39,40], mainly due to the strengthening of ocean stratification under global warming[15]. However, with the continuous increase in NO_x emissions, the higher efficiency of NO_3^- formation in the MABL of the NH will increase the contribution of atmospheric deposition to ocean productivity, especially in persistently N-limited regions such as the North Atlantic Subtropical Gyres[15]. Therefore, the marine ecological effects of atmospheric deposition should be given more attention in the future, especially in remote oligotrophic oceans.

Methods

Field sampling

Total suspended particulates (TSP) in the MABL were collected in pre-combusted (450 °C for 4 h) microquartz fibre filters (203 × 254 mm, Munktell, Sweden) using a high-volume air sampler (flow rate: 1.05–1.34 m^3 min^{-1}, KB-1000-180815, Xiamen, China) during the Northwest Pacific and Indian Ocean cruises (Supplementary Fig. 5) aboard the R/V Xiangyanghong 06. The sampler during these two cruises was placed on the top deck and the front of the scientific research vessel at 3 m above sea level. The Indian Ocean cruise was conducted from the coast of Eastern China (Shanghai, China; 29.95°N, 122.18°E), through the South China Sea, to the northern Indian Ocean (3.00°S, 91.50°E), from November 2019 to March 2020. A Northwest Pacific cruise was conducted from the coast of Eastern China (Shanghai, 29.90°N, 122.22°E) to the Northwest Pacific Ocean (3.11°N, 155.95°E) between December 2020 and February 2021. A total of

26 and 15 TSP samples were collected during the Indian Ocean and Northwest Pacific Ocean cruises, respectively (Supplementary Table 1).

TSP samples were collected in precombusted (450 °C for 4 h) polytetrafluoroethylene membranes (90-mm diameter, Whatman) using TH-150A intelligent volumetric samplers (Wuhan Tianhong Intelligent Instruments, Inc., Wuhan, China, flow rate: 0.10 m^3 min^{-1}) during the Arctic cruise, which was placed on the top deck and the front of the Chinese icebreaker RV *Xuelong* at 3 m above sea level. The Arctic cruise was conducted from the Northwest Pacific Ocean (42.32°N, 136.75°E) to the Arctic Ocean (86.04°N, 161.85°W) during the 11th Chinese Arctic Research Expedition (CHINARE) from July to September 2020. A total of 14 TSP samples were collected during the Arctic cruise. In addition, a total of 2, 3, and 2 field blanks were collected during the Northwest Pacific Ocean, Indian Ocean, and Arctic cruises, respectively. Clean pre-combusted filters installed in the air sampler without pumping were considered field blank samples for the three cruises. After sampling, the TSP and field black samples were wrapped in aluminium foil and stored under −20 °C in the laboratory.

To avoid contamination from the scientific research vessel exhaust, the sampler was operated only under conditions where the relative wind direction was within ±90° of the bow and the wind speed was higher than 1 m s^{-1} during those three cruises. Sampling duration for each aerosol sample was 48–168 h during the Northwest Pacific and Indian Ocean cruises, and was 33–95 h during the Arctic cruise. Detailed sampling information is presented in Supplementary Table 1.

Sample treatment and analysis

The procedure for extracting NO_3^- and its oxygen isotopes was followed as described in a previous study[41]. Samples for the Indian Ocean and Northwest Pacific cruises and 1/8 filters were extracted with 30 mL of ultrapure water and shaken for 30 min. For the Arctic cruise, all filter samples were extracted using similar processes owing to the smaller filters. The extraction procedure was repeated thrice, and all the extraction solutions for each sample were transferred to a pre-cleaned polyethene plastic bottle and diluted to 100 mL with ultrapure water. The extraction solutions were filtered by a GF/F membrane (0.7-μm-pore-size, 47 mm diameter, Millipore) for NO_3^- and its oxygen isotope measurements.

NO_3^- concentrations in the extraction solutions were measured using a San++ continuous flow analyser (Skalar, Netherlands). The detection limit for NO_3^- measurement was 0.1 μmol L^{-1}. Finally, the measured NO_3^- concentration is converted to gas volume concentration (μmol L^{-1}) based on the sampling volume of air sampled (m^3) and the volume of extraction solutions (L). In this study, NO_3^- concentrations in the blank field samples were found to be all below the detection limit.

The composition of oxygen isotope ($\delta^{18}O$-NO_3^-) was measured using a chemical method (cadmium-azide) modified from McIlvin and Altabet[42], and the detailed analysis procedure can be found in our previous study[41]. In the extraction solutions, NO_3^- was firstly removed by sulfamic acid, and then NO_3^- was reduced to nitrite (NO_2^-) by adding spongy Cd. NO_2^- was further reduced to nitrous oxide by sodium azide in an acetic acid buffer, and then nitrous oxide was separated and determined for $\delta^{18}O$-NO_3^- using a Precon-GasBench II-253 plus (Thermo Scientific, United States). The composition of $\delta^{18}O$-NO_3^- was calibrated using the international standard of the International Atomic Energy Agency (IAEA)-N3, and the reproducibility of duplicate analysis was <0.6‰, with a mean of ±0.3‰.

Literature and open-source data

To comprehensively evaluate the mechanism of NO_3^- formation in the global marine boundary layer, NO_3^- and its oxygen isotope data were collected from five other cruises in the Atlantic[24], Antarctic[17], Western-Central Pacific Ocean[30], and Eastern Pacific Ocean[34,43] (Supplementary Fig. 5). An Antarctic cruise was conducted from the coast of Eastern China to the Southern Ocean (69.37°S, 76.37°E) from November 2015 to April 2016 during the 32nd CHINARE. The Eastern Pacific Ocean-G15 cruise was conducted along the Eastern Pacific latitude (55.1°N, 155.7°W-20.0°S, 152.0°W) from 20 September to 22 November 2018. The Eastern Pacific Ocean-G16 cruise was conducted along the Eastern Pacific with longitude (from 4.07°S, 81.90°W to 10.50°S, 152.00°W) from 26 October to 16 December 2013. Atlantic cruises were conducted in the Weddell Sea area from 05 September 2006 to 28 October 2006 and between Cape Town (South Africa) and Bremerhaven (Germany) from 13 April 2007 to 03 May 2007. Western Central Pacific cruises were conducted from Japan to New Zealand (37°S, 172°W) from 11 December 2013 to 12 February 2014 and the North Pacific Ocean from 23 June to 11 August 2014. All eight cruises were conducted over the open oceans, which are less directly affected by human activities. Therefore, the NO_3^- isotopes reflect the transformation processes of NO_3^- in the MABL.

Calculation of day length

The calculation of day length was primarily based on the solar altitude angle[22]. The formula used was as follows:

$$PD = 90^\circ - SAA \quad (1)$$

$$DDL = 12h/PD \quad (2)$$

$$DL = 12h + (DDL \times L) \quad (3)$$

where, PD represents the latitude of the polar day, SAA represents the solar altitude angle, DDL represents the difference in day length at different latitudes, DL represents the day length at a certain latitude, and L represents the value at that latitude. This study assumed that the moving speed of the solar altitude angle from the Equator to the Tropic of Cancer (23.4333°N) (93 d from 21 March to 21 June) and the Tropic of Cancer (93 d from 22 June to 22 September) was 0.252°/d (23.4333°/93 d). The speed from the Equator to the Tropic of Capricorn (23.4333°S) (90 d from 23 September to 21 December) and the Tropic of Capricorn to the Equator (89 d from 22 December to 20 March) were 0.260°/d (23.4333°/90 d) and 0.263°/d (23.4333°/89 d), respectively. The variations in day length by month in the SH and NH groups are shown in Supplementary Fig. S2.

Data processing

Research on NO_3^- in global ocean aerosols remains limited because it is challenging to conduct marine field surveys. In this study, in addition to the samples collected from our three cruises (Indian Ocean cruise, Northwest Pacific cruise and Arctic cruise), we also collected data from other cruises. Due to the focus of this study on the formation process of NO_3^- in the global MABL, the influence of sources on nitrate oxygen isotopes is less[27]. Therefore, even if the sampling periods of these cruises differed, we could still merge them to discuss the mechanism of hemispherical scale formation. However, aerosol NO_3^- concentrations typically exhibit significant seasonal variations in continental and coastal waters, particularly in areas affected by monsoons. This is because the monsoon conversion directly determines the input of pollution sources. This influence gradually weakens toward the sea and becomes less significant in the open ocean, as these areas are far from land and are less affected by the monsoon[17,44]. Therefore, to calculate the global average concentration of marine aerosols, this study removed the concentration in coastal areas that are susceptible to monsoon influence, and the final result reflects the concentration of aerosol NO_3^- in open-sea areas, which can reduce the impact of different sampling periods on the voyages.

Statistical information

Pearson correlation analyses (Figs. 2 and 3) were performed using the SPSS 19.0 statistical package (SPSS Inc., Chicago, IL, USA) and Origin 2022 statistical package (OriginLab Corporation, USA). The average values and standard deviations (SD) are reported.

Data availability

This article presents the data underlying the results of this study. The source data are provided in this paper.

Code availability

The codes to reproduce the analyses presented in this study are available upon request from the corresponding author.

Received: 8 March 2024; Accepted: 11 June 2024;
Published online: 18 June 2024

References

1. Ye, C. et al. Rapid cycling of reactive nitrogen in the marine boundary layer. *Nature* **532**, 489–491 (2016).
2. Miyazaki, K. et al. Decadal changes in global surface NOx emissions from multi-constituent satellite data assimilation. *Atmos. Chem. Phys.* **17**, 807–837 (2017).
3. Crippa, M. et al. Forty years of improvements in European air quality: regional policy-industry interactions with global impacts. *Atmos. Chem. Phys.* **16**, 3825–3841 (2016).
4. Song, W. et al. Important contributions of non-fossil fuel nitrogen oxides emissions. *Nat. commun.* **12**, 243 (2021).
5. Chen, Z. L. et al. Significant contributions of combustion-related sources to ammonia emissions. *Nat. Commun.* **13**, 7710 (2022).
6. Liu, X. et al. Enhanced nitrogen deposition over China. *Nature* **494**, 459–462 (2013).
7. Hastings, M. G., Jarvis, J. C. & Steig, E. J. Anthropogenic impacts on nitrogen isotopes of ice-core nitrate. *Science* **324**, 1288–1288 (2009).
8. Finlayson-Pitts, B. J., Pitts Jr J. N. *Chemistry of the upper and lower atmosphere: theory, experiments, and applications* (Elsevier, 1999).
9. Duce, R. A. et al. Impacts of atmospheric anthropogenic nitrogen on the open ocean. *Science* **320**, 893–897 (2008).
10. Altieri, K. E., Fawcett, S. E. & Hastings, M. G. Reactive nitrogen cycling in the atmosphere and ocean. *Annu. Rev. Earth Pl. Sc.* **49**, 523–550 (2021).
11. Renforth, P. & Henderson, G. Assessing ocean alkalinity for carbon sequestration. *Rev. Geophys.* **55**, 636–674 (2017).
12. Krause-Jensen, D. & Duarte, C. M. Substantial role of macroalgae in marine carbon sequestration. *Nat. Geosci.* **9**, 737–742 (2016).
13. Reay, D. S., Dentener, F., Smith, P., Grace, J. & Feely, R. A. Global nitrogen deposition and carbon sinks. *Nat. Geosci.* **1**, 430–437 (2008).
14. Hutchins, D. A. & Capone, D. G. The marine nitrogen cycle: new developments and global change. *Nat. Rev. Microbiol.* **20**, 401–414 (2022).
15. Dai, M. et al. Upper ocean biogeochemistry of the oligotrophic North Pacific Subtropical Gyre: from nutrient sources to carbon export. *Rev. Geophys.* **61**, e2022RG000800 (2023).
16. Prospero, J. M. & Savoie, D. L. Effect of continental sources on nitrate concentrations over the Pacific Ocean. *Nature* **339**, 687–689 (1989).
17. Shi, G. et al. Using stable isotopes to distinguish atmospheric nitrate production and its contribution to the surface ocean across hemispheres. *Earth Planet. Sci. Lett.* **564**, 116914 (2021).
18. Alexander, B. et al. Quantifying atmospheric nitrate formation pathways based on a global model of the oxygen isotopic composition ($\Delta^{17}O$) of atmospheric nitrate. *Atmos. Chem. Phys.* **9**, 5043–5056 (2009).
19. Alexander, B. et al. Global inorganic nitrate production mechanisms: comparison of a global model with nitrate isotope observations. *Atmos. Chem. Phys.* **20**, 3859–3877 (2020).
20. Schmidt, J. A. et al. Modeling the observed tropospheric BrO background: Importance of multiphase chemistry and implications for ozone, OH, and mercury. *J. Geophys. Res. Atmos.* **121**, 11–819 (2016).
21. Lelieveld, J., Gromov, S., Pozzer, A. & Taraborrelli, D. Global tropospheric hydroxyl distribution, budget and reactivity. *Atmos. Chem. Phys.* **16**, 12477–12493 (2016).
22. Luo, L. et al. Quantifying the formation pathways of nitrate in size-segregated aerosols during winter haze pollution. *Gondwana Res.* **115**, 71–80 (2023).
23. Savarino, J. et al. Isotopic composition of atmospheric nitrate in a tropical marine boundary layer. *Proc. Natl Acad. Sci.* **110**, 17668–17673 (2013).
24. Morin, S. et al. Comprehensive isotopic composition of atmospheric nitrate in the Atlantic Ocean boundary layer from 65 S to 79 N. *J. Geophys. Res. Atmos.* **114**, D05303 (2009).
25. Vicars, W. C. & Savarino, J. Quantitative constraints on the ^{17}O-excess ($\Delta^{17}O$) signature of surface ozone: Ambient measurements from 50N to 50S using the nitrite-coated filter technique. *Geochim. Cosmochim. Acta* **135**, 270–287 (2014).
26. Krankowsky, D. et al. Measurement of heavy isotope enrichment in tropospheric ozone. *Geophys. Res. Lett.* **22**, 1713–1716 (1995).
27. Morin, S. et al. Tracing the origin and fate of NOx in the Arctic atmosphere using stable isotopes in nitrate. *Science* **322**, 730–732 (2008).
28. Theys, N. et al. Global observations of tropospheric BrO columns using GOME-2 satellite data. *Atmos. Chem. Phys.* **11**, 1791–1811 (2011).
29. Richter, A., Wittrock, F., Ladstätter-Weißenmayer, A. & Burrows, J. P. GOME measurements of stratospheric and tropospheric BrO. *Adv. Space Res.* **29**, 1667–1672 (2002).
30. Kamezaki, K. et al. Tracing the sources and formation pathways of atmospheric particulate nitrate over the Pacific Ocean using stable isotopes. *Atmos. Environ.* **209**, 152–166 (2019).
31. Gligorovski, S., Strekowski, R., Barbati, S. & Vione, D. Environmental implications of hydroxyl radicals (• OH). *Chem. Rev.* **115**, 13051–13092 (2015).
32. Pfannerstill, E. Y. et al. Total OH reactivity over the Amazon rainforest: variability with temperature, wind, rain, altitude, time of day, season, and an overall budget closure. *Atmos. Chem. Phys.* **2020**, 1–42 (2020).
33. Wang, H. et al. Increased night-time oxidation over China despite widespread decrease across the globe. *Nat. Geosci.* **16**, 217–223 (2023).
34. Joyce, E. E., Balint, S. J. & Hastings, M. G. Isotopic evidence that alkyl nitrates are important to aerosol nitrate formation in the Equatorial Pacific. *Geophys. Res. Lett.* **49**, e2022GL099960 (2022).
35. Friedel, M. et al. Springtime arctic ozone depletion forces northern hemisphere climate anomalies. *Nat. Geosci.* **15**, 541–547 (2022).
36. Bates, T. S., Coffman, D. J., Covert, D. S. & Quinn, P. K. Regional marine boundary layer aerosol size distributions in the Indian, Atlantic, and Pacific Oceans: A comparison of INDOEX measurements with ACE-1, ACE-2, and Aerosols99. *J. Geophys. Res. -Atmos.* **107**, INX2–25 (2002).
37. Fang, Y. T. et al. Anthropogenic imprints on nitrogen and oxygen isotopic composition of precipitation nitrate in a nitrogen-polluted city in southern China. *Atmos. Chem. Phys.* **11**, 1313–1325 (2011).
38. Brean, J. et al. Open ocean and coastal new particle formation from sulfuric acid and amines around the Antarctic Peninsula. *Nat. Geosci.* **14**, 383–388 (2021).
39. Boyce, D. G., Lewis, M. R. & Worm, B. Global phytoplankton decline over the past century. *Nature* **466**, 591–596 (2010).
40. Polovina, J. J., Howell, E. A. & Abecassis, M. Ocean's least productive waters are expanding. *Geophys. Res. Lett.* **35**, 618 (2008).
41. Luo, H. et al. Nitrate sources and formation in aerosol and precipitation in a tropical city in South China: Insight from nitrate dual isotopes. *Atmos. Environ.* **278**, 119087 (2022).
42. McIlvin, M. R. & Altabet, M. A. Chemical conversion of nitrate and nitrite to nitrous oxide for nitrogen and oxygen isotopic analysis in freshwater and seawater. *Anal. Chem.* **77**, 5589–5595 (2005).
43. Carter, T. T. S., Joyce, E. E. & Hastings, M. G. Quantifying Nitrate Formation Pathways in the Equatorial Pacific Atmosphere from the GEOTRACES Peru-Tahiti Transect. *ACS Earth Space Chem.* **5**, 2638–2651 (2021).

44. Prospero, J. M., Savoie, D. L., Nees, R. T., Duce, R. A. & Merrill, J. Particulate sulfate and nitrate in the boundary layer over the North Pacific Ocean. *J. Geophys. Res. Atmos.* **90**, 10586–10596 (1985).

Acknowledgements

This study was supported by the National Natural Science Foundation of China (U1901213, 92158201, 42276047, 42176039), Global Change and Air-Sea Interaction II Program (GASI-01-EIND-STwin), and Innovation and Entrepreneurship Project of Shantou (2021112176541391).

Author contributions

Q.L. processed the data, and wrote the manuscript. Q.L. and F.C. conceived the idea and designed the study. F.C., H.L., J.Y., and Z.L. provided key suggestions on this work, and helped to improve the design of the figures. G.H., C.C., and Q.Z. assisted in the data analysis. Q.L., H.L., J.Y., G.H., Z.L., C.C., Q.Z., and F.C. discussed the results and contributed to the final manuscript.

Competing interests

The authors declare no competing interest.

Additional information

Supplementary information The online version contains supplementary material available at https://doi.org/10.1038/s41612-024-00694-2.

Correspondence and requests for materials should be addressed to Fajin Chen.